Developmental Biology 374 (2013) 185–197

Contents lists available at SciVerse ScienceDirect

Developmental Biology

journal homepage: www.elsevier.com/locate/developmentalbiology

Evolution of Developmental Control Mechanisms

Fgf8 dosage determines midfacial integration and polarity within the nasal and optic capsules

John N. Griffin [a,1], Claudia Compagnucci [a], Diane Hu [b], Jennifer Fish [a,c], Ophir Klein [d], Ralph Marcucio [b], Michael J. Depew [a,b,*]

[a] Dept. of Craniofacial Development, King's College London, Floor 27, Guy's Hospital, London Bridge, London SE1 9RT, UK
[b] Department of Orthopaedic Surgery, UCSF, 2550 24th Street, SFGH Bldg 9, Room 346, San Francisco, CA 94110, USA
[c] Department of Orthopaedic Surgery, UCSF, 513 Parnassus Avenue, Medical Sciences Bldg. S-1161, San Francisco, CA 94143, USA
[d] Departments of Orofacial Sciences and Pediatrics, Institute for Human Genetics and Program in Craniofacial and Mesenchymal Biology, UCSF, 513 Parnassus Avenue, San Francisco, CA 94143-0442, USA

ARTICLE INFO

Article history:
Received 23 February 2012
Received in revised form
24 October 2012
Accepted 15 November 2012
Available online 29 November 2012

Keywords:
Fgf8
Nasal capsule
Optic capsule
Mouse
Ectoderm
Midface
Craniofacial
Trabecular basal plate
FEZ

ABSTRACT

Craniofacial development requires an exquisitely timed and positioned cross-talk between the embryonic cephalic epithelia and mesenchyme. This cross-talk underlies the precise translation of patterning processes and information into distinct, appropriate skeletal morphologies. The molecular and cellular dialogue includes communication via secreted signaling molecules, including *Fgf8*, and effectors of their interpretation. Herein, we use genetic attenuation of *Fgf8* in mice and perform gain-of-function mouse-chick chimeric experiments to demonstrate that significant character states of the frontonasal and optic skeletons are dependent on *Fgf8*. Notably, we show that the normal orientation and polarity of the nasal capsules and their developing primordia are dependent on *Fgf8*. We further demonstrate that *Fgf8* is required for midfacial integration, and provide evidence for a role for *Fgf8* in optic capsular development. Taken together, our data highlight *Fgf8* signaling in craniofacial development as a plausible target for evolutionary selective pressures.

Introduction

The appropriate patterning, morphogenesis and integration of the gnathostome skull are achieved via an exquisitely positioned and timed cross-talk between the embryonic cephalic epithelia and the subjacent mesenchyme. Elaboration of this cross-talk is manifested in the induction and maintenance of intricate patterns of gene expression, the spatial and temporal details of which underlie the precise translation of patterning processes and information into discrete, appropriate skeletal morphologies. The lambdoidal junction (λ-junction), formed where the maxillary division of the first branchial arch (mxBA1) meets the medial (mFNP) and lateral (lFNP) frontonasal processes, exemplifies a morphologically and molecularly intricate epithelial–mesenchymal craniofacial interface (Depew and Compagnucci, 2008; Compagnucci et al., 2011). The organization of the λ-junction is complex and embodies the future positions of the choanae, the upper lips and (premaxillary) incisors, the primary and secondary palates, and the optic (OPC) and nasal (NSC) capsules (Fig. 1). The functionality and morphology of each of these structures depends on the appropriate orientation and polarity (i.e., relative development along the medio-lateral, dorso-ventral and rostro-caudal axes) of the craniofacial primordia associated with the λ-junction during development (Tamarin and Boyde, 1977; Compagnucci et al., 2011).

Outside of enamel-producing ameloblasts, cephalic epithelia do not yield cranial skeletal structures: The importance of these epithelial cells to cranial skeletal morphology and evolution thus largely lies in their influences on the mesenchyme, much of it cranial neural crest (CNC) in origin. Phenotypic analyses of mutations of genes expressed in the ectoderm (and not the associated CNC) have demonstrated the requirement for a properly informed and competent surface cephalic ectoderm (SCE) (Depew and Compagnucci, 2008). Extirpation studies indicate that the olfactory placode is essential to the formation of the NSC: Without an olfactory placode, the morphologic events surrounding the formation of the olfactory pits (OFP) fail to manifest and a knock-on effect on the skeleton of the capsule ensues (Bell, 1907;

* Corresponding author
E-mail addresses: michael.j.depew@gmail.com, depewm@orthosurg.ucsf.edu (M.J. Depew).
[1] Current Address: Department of Pediatrics, Yale University School of Medicine, New Haven, CT, USA.

0012-1606/$ - see front matter © 2012 Elsevier Inc. All rights reserved.
http://dx.doi.org/10.1016/j.ydbio.2012.11.014

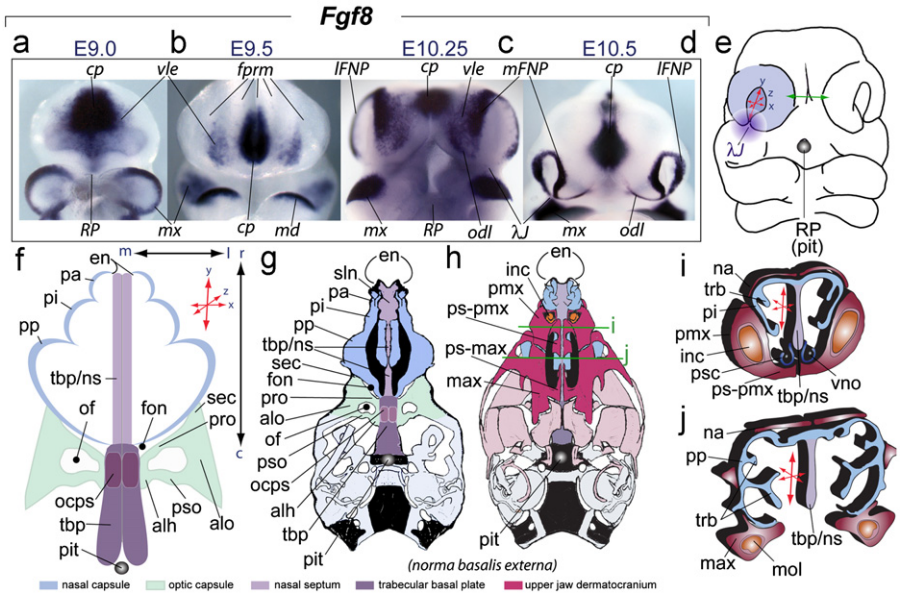

Fig. 1. Elaboration of frontonasal *Fgf8* expression, its relation to the λ-junction, and the structural orientation and polarity of the frontonasal skeleton. (a)–(d) In situ hybridization of *Fgf8* in the SCE and frontonasal region from E9 to E10.5. The mandibular first arches in 'a' and 'c' have been removed to better view the ventrolateral ectoderm (vle). (e) Diagram of an E10.5 murine embryo showing inherent polarity (here defined as relative elaboration along the rostro-caudal, medio-lateral and dorso-ventral axes (represented by 'x:y:z' coordinate red arrows) of the olfactory pit. Green arrows highlight the fact that contra-lateral mFNPs must eventually conjoin across the midline. Purple gradient disc: central rami of the λ-junction (λJ) (after Compagnucci et al., 2011). Grey-scale circle: the position of Rathke's Pouch (RP) that yields the pituitary (pit) which demarcates the position of caudal boundary of the trabecular basal plate (TBP). (f)–(i′) Diagrams of the developing skeleton associated with the nasal capsule (NSC), optic capsule (OPC), and midline skeleton of the neurocranium and their orientation and polarity. (f) The three pars of the NSC are in blue, the TBP (midline) structures in shades of purple, and the OPC in green. (g) and (h) Schemae of *norma basalis externa* views of neonatal murine skulls. Blue: NSC structure. Purple: TBP midline structures and the red: upper jaw dermatocranium. Green lines: the relative positions of the coronal sections for "i" and "j". (i) and (j) Nature of NSC polarity as depicted in diagrams of coronal sections of a murine skull. (For interpretation of the references to color in this figure legend, the reader is referred to the web version of this article).

Burr, 1916; Corsin, 1971; Reiss, 1998; Schmalhausen, 1939; Toerien and Roussouw, 1977; Zwilling, 1940). Hence, formation of the placode and its subsequent subdivision is essential to the parsing of regional pattern and structure, though the specifics of the correlation between aberrant olfactory placodogenesis and loss of NSC structure or bi-capsular integration with the midline trabecular basal plate (TBP) has yet to be fully understood. Furthermore, manipulations of avian SCE have identified a sub-region, the facial ectodermal zone, or FEZ, and factors expressed therein (e.g., *Shh*, *Bmp4*, and *Fgf8*), as critical for the development of sub-components of the associated skeleton (Hu et al., 2003; Marcucio et al., 2005). Specifically, the FEZ regulates proximo-distal extension and dorso-ventral polarity of the middle part of the upper jaw (Hu et al., 2003, Hu and Marcucio, 2009).

Fgf8 is dynamically expressed during SCE ontogeny (Fig. 1), and has been shown to regulate specific aspects of craniofacial pattern and development (Abu-Issa et al., 2002; Bailey et al., 2006; Creuzet et al., 2004; Crossley and Martin, 1995; Depew et al., 2002b; Dode and Hardelin, 2009; Ferguson et al., 2000; Frank et al., 2002; Hu et al., 2003; Kawauchi et al., 2005; Lioubinski et al., 2006; Macatee et al., 2003; Neubüser et al., 1997; Pauws and Stanier, 2007; Riley et al., 2007; Storm et al., 2006; Szabo-Rogers et al., 2008; Trumpp et al., 1999; Tucker et al., 1999a, 1999b). Mice which have lost *Fgf8* in the SCE due to conditional inactivation of a floxed allele (Kawauchi et al., 2005) or which carry hypomorphic alleles of *Fgf8* (Abu-Issa et al., 2002; Frank et al., 2002) demonstrate its necessity for olfactory placodogenesis. Moreover, over- and under-expression studies have shown *Fgf8* to affect the development of the avian craniofacial skeleton (Abzhanov and Tabin, 2004; Szabo-Rogers et al., 2008). Cumulative evidence therefore indicates that the elaborate ontogeny of *Fgf8* expression in the SCE reflects a dynamic and significant signaling environment to be encountered by the CNC responsible for generating rostral cranial skeletal structures.

We have previously proposed that, just as artificial modulation of *Fgf8* levels in the SCE through experimentation results in altered skeletal morphologies, modulation of *Fgf8* levels through natural selection may have acted as an evolutionary means of generating variation in cranial skeletal morphologies (Depew and Simpson, 2006; Depew and Compagnucci, 2008). To address the relationship between levels of *Fgf8* signaling and the complex cranial skeleton of the rostral head, we have used several approaches to vary Fgf8 levels in the SCE. We have utilized combinations of previously characterized hypomorphic (*Neo*) and null murine *Fgf8* alleles to allow for a modulation of *Fgf8* signaling by reducing functional expression levels to approximately 20% ($Fgf8^{null/Neo}$), 40% ($Fgf8^{Neo/Neo}$), 50% ($Fgf8^{+/null}$) or 70% ($Fgf8^{+/Neo}$) of normal (wild-type) levels (for characterizations of alleles and relative levels of Fgf8 protein, see Meyers et al., 1998; Abu-Issa et al., 2002; Frank et al., 2002; Storm et al., 2003, 2006). These graded challenges to *Fgf8*-regulated cranial morphogenesis allowed us to demonstrate that *Fgf8* dosage determines murine mid-facial integration and polarity within the NSC and OPC. We have additionally used wild-type and *Fgf8*-compromised murine SCE in murine-chick xenograft experiments to show that differential *Fgf8* allelic dosages elicit disparate responses in host tissue, further suggesting that patterning and growth are dosage dependent.

Materials and methods

Murine anatomical analyses. $Fgf8^{+/+}$, $Fgf8^{+/Neo}$, $Fgf8^{+/null}$, $Fgf8^{Neo/Neo}$ and $Fgf8^{null/Neo}$ mice perinates were collected, rinsed in PBS, and photographed. Differential staining of bone and cartilage in neonates followed established protocols (Depew, 2008).

Whole mount in situ hybridization, TUNEL and proliferation assays. Embryos were fixed overnight in 4% paraformaldehyde (PFA) in PBS at 4 °C, rinsed, and passed through a grades series of MeOH. Whole mount in situ hybridization and preparation of *Alx3*,

Alx4, *Barx2*, *Bmp4*, *Dlx2*, *Dlx5*, *Fgf8*, *Msx1*, *Msx2*, *Pea3*, *Pitx1*, *Raldh3*, *Satb2*, *Six1*, *Spry1*, *Tbx3*, and *Wnt5a* ribroprobes followed standard protocols as described in Depew et al., 1999. Unless otherwise noted, multiple embryos were used for each experimental parameter. Apoptotic cells were detected in whole mount embryos by terminal transferase dUTP-biotin nick-end labeling (TUNEL) using a kit (in situ cell death detection kit, Roche cat#11684795910) following the manufacturer's instructions. Sections were counterstained with Hoechst dye. Whole mount apoptotic cell death was assessed by TUNEL assay on E10.5 embryos using an Apoptag Peroxidase in situ apoptosis detection kit (Chemicon) as per manufacturer's instructions. Proliferation rates were assayed through immunohistochemical analysis of sections stained with an anti-phosphohistone H3 antibody (Cellsignal, cat# #9701, at a 1:200 dilution with antigen retrieval in Sodium Citrate buffer at 100 °C for 25 min) and counterstained with DAPI.

Scanning electron microscopy. Embryos from timed pregnancies were harvested and fixed at 4 °C overnight in 4% paraformaldehyde and 0.2% glutaraldehyde, washed in PBS, dehydrated in a graded ethanol series, critical point dried, sputter coated with gold, and viewed and photographed in a FEI Quanta FEG operating at 10 kV.

Mouse–chick chimeras. Wild-type and $Fgf8^{null/Neo}$ embryos were harvested at E10.5 and FEZ ectodermal grafts were prepared as per Hu et al., 2003 and Hu and Marcucio, 2009. Chick embryos were incubated to HH25 and used as hosts for engraftment of the FEZ from mutant and wild-type mice as described (Hu and Marcucio, 2009). 1 ml of albumin was removed and a small hole was made in the shell to expose the embryo. Then host ectoderm was removed from an area corresponding to the size of the graft tissue, and the murine ectoderm was placed and secured onto the prepared host site with glass pins (Fig. 7). Mouse–chick chimeras were incubated until day 13, photographed, and fixed in 4% paraformaldehyde, dehydrated, embedded in paraffin, sectioned, and stained with safranin-O and Fast green.

Animal genotyping. As per Meyers et al., 1998.

Results

Fgf8 dosage determines polarity and orientation within the nasal and optic capsules and midfacial integration

To determine whether cranial skeletal morphology associated with the λ-junction is sensitive to allelic dosage of *Fgf8* we examined perinatal $Fgf8^{+/+}$, $Fgf8^{+/Neo}$, $Fgf8^{+/null}$, $Fgf8^{Neo/Neo}$ and $Fgf8^{null/Neo}$ mice differentially stained for bone and cartilage (Fig. 2). $Fgf8^{null/null}$ embryos die from defective gastrulation (Sun et al., 1999) and were therefore unexamined. Confirming previous reports (Meyers et al., 1998), we found that neonatal $Fgf8^{+/Neo}$ and $Fgf8^{+/null}$ mice were phenotypically comparable to wild-type littermates (Fig. 2b). $Fgf8^{Neo/Neo}$ neonates exhibited altered NSC ($n=4/8$) and OPC ($n=8/8$), as well as TBP ($n=4/8$) to which they both attach, while $Fgf8^{null/Neo}$ mutants evinced more drastic alterations still ($n=14/14$), typically exhibiting midfacial cleft ($n=12/14$; Fig. 2a1, d, g–l, k), among which a few ($n=2/12$) were found to have a clearly split mid-face but some midline facial tissue still apposed (Fig. 2a2, j, l). Atypically, a perinatal $Fgf8^{null/Neo}$ mutant exhibited an oro-rhinarial asymmetry or presented with a loss of the rhinarium altogether ($n=2/14$) wherein such animals showed a near complete collapse of structure centered at the midline (Fig. 2a3,4, d4). To present the cranial skeletal structural changes of the $Fgf8^{Neo/Neo}$ and $Fgf8^{null/Neo}$ neonates (concentrating on the great majority ($n=12/14$), or 'typical', phenotype encountered), we describe and compare them to phenotypically wild-type littermates (either $Fgf8^{+/+}$ or $Fgf8^{+/null}$) by region below.

Optic Capsules. OPC contain two struts, the pre-optic and post-optic pillars, that run laterally from the TBP to a third component, the ala orbitalis, a cartilaginous wing representing the lateral boundary support to the optic apparatus that normally connects the OPC (rostrad) to the NSC (via the sphenethmoidal commissure) and (caudad) the taenia marginalis (Figs. 1 and 2); together, the pre-optic pillar, post-optic pillar, ala orbitalis and TBP enclose the optic foramen. In $Fgf8^{Neo/Neo}$ neonates, the ala orbitalis did not appropriately expand laterad and attached only to the pre-optic pillar, itself abnormally represented by a cylindrical rod mis-oriented caudo-laterally ($n=8/8$; Fig. 2c). The $Fgf8^{Neo/Neo}$ sphenethmoidal commissures extended rostrad but were smaller and mis-oriented toward the middle of the pars posteriors of the NSCs. Each mutant post-optic pillar was hypoplastic, with only a precociously ossifying remnant of the ala hypochiasmatica remaining (Fig. 2c). Thus, a true optic foramen failed to form.

These structural changes were exacerbated in the $Fgf8^{null/Neo}$ neonates ($n=14/14$), with the ala orbitalis even further reduced in size and its sphenethmoidal commissure extension noticeably smaller (Fig. 2d, g–l). Notably, directional asymmetry (consistent sidedness) existed in the remnants of the ala hypochiasmatica of $Fgf8^{null/Neo}$ neonates as the *right* side was typically larger and more robust ($n=10/14$) (Fig. 2d, h, j, l, where the skulls presented are viewed from below and hence the right side of the skull appears on the left side of the picture). This represents the first demonstration that *Fgf8* is essential for normal OPC development and that capsular morphogenesis is *Fgf8* dosage sensitive.

Nasal Capsules. NSCs are complex structures grossly composed of three subdivisions (Figs. 1 and 2; Depew et al., 2002b). The rostral-most component, through which the external nares provides entrance to the NSC (and cavity), is the pars anterior; just caudal to this is a medial subdivision, the pars intermedia, which is followed by the caudal-most pars posterior. The TBP and its nasal septal extension form the medial, midline boundaries of the NSC.

Compared to wild-types (or $Fgf8^{+/null}$), the NSC of affected $Fgf8^{Neo/Neo}$ neonates ($n=4/8$) were slightly hypoplastic rostrally with both the pars anterior and pars intermedia compressed toward the midline (Fig. 2c); the anterior of the pars posterior of $Fgf8^{Neo/Neo}$ skulls extended laterad, as with wild-types, but the posterior ends, as represented by the cupola nasi posterior, were hypoplastic and did not fully come together with their contra-lateral partners at the midline. Turbinalia, scroll-like projections from the interior of the NSC, were present but hypoplastic in $Fgf8^{Neo/Neo}$ neonatal mutants.

Alterations of the NSC of $Fgf8^{null/Neo}$ neonates were substantially more extensive than those seen in $Fgf8^{Neo/Neo}$ neonates, and represented a significant change in the orientation and polarity of NSC structure ($n=14/14$) (Fig. 2d, h–l). Contra-lateral NSC did not meet at the midline but were integrated with bilaterally separated nasal septa ($n=12/14$). The pars anterior were severely hypoplastic (rostro-caudally, dorso-ventrally and medio-laterally), lacked developed alae and crista semicirculari, and possessed aberrant naral openings. Mutant pars intermedia were compressed rostro-caudally but slightly expanded medio-laterally, lacking proper capsular floors (solum nasi). Paraseptal cartilages were not present. The pars psoterior presented an extensive lateral expansion and enlargement of the recessus cupularis at their anterior ends, and maintained the processus maxillaris that extends externally from the posterior margin of the recessus cupularis. However, the pars posterior evinced an extensive hypoplasia of the cupola nasi posterior, which only presented as cartilaginous spurs oriented toward the base of the split nasal septum (Fig. 2h). Fenestra basinasali were present but were pushed rostrad. Ethmoturbinalia were either hypoplastic or missing, the cribriform plates being smaller and less fenestrated. Asymmetry between the contra-lateral NSC was occasionally encountered, generally being more acute rostrally within the pars anterior and pars intermedia ($n=4/14$; Fig. 2j, k); however, unlike with the OPC, directional

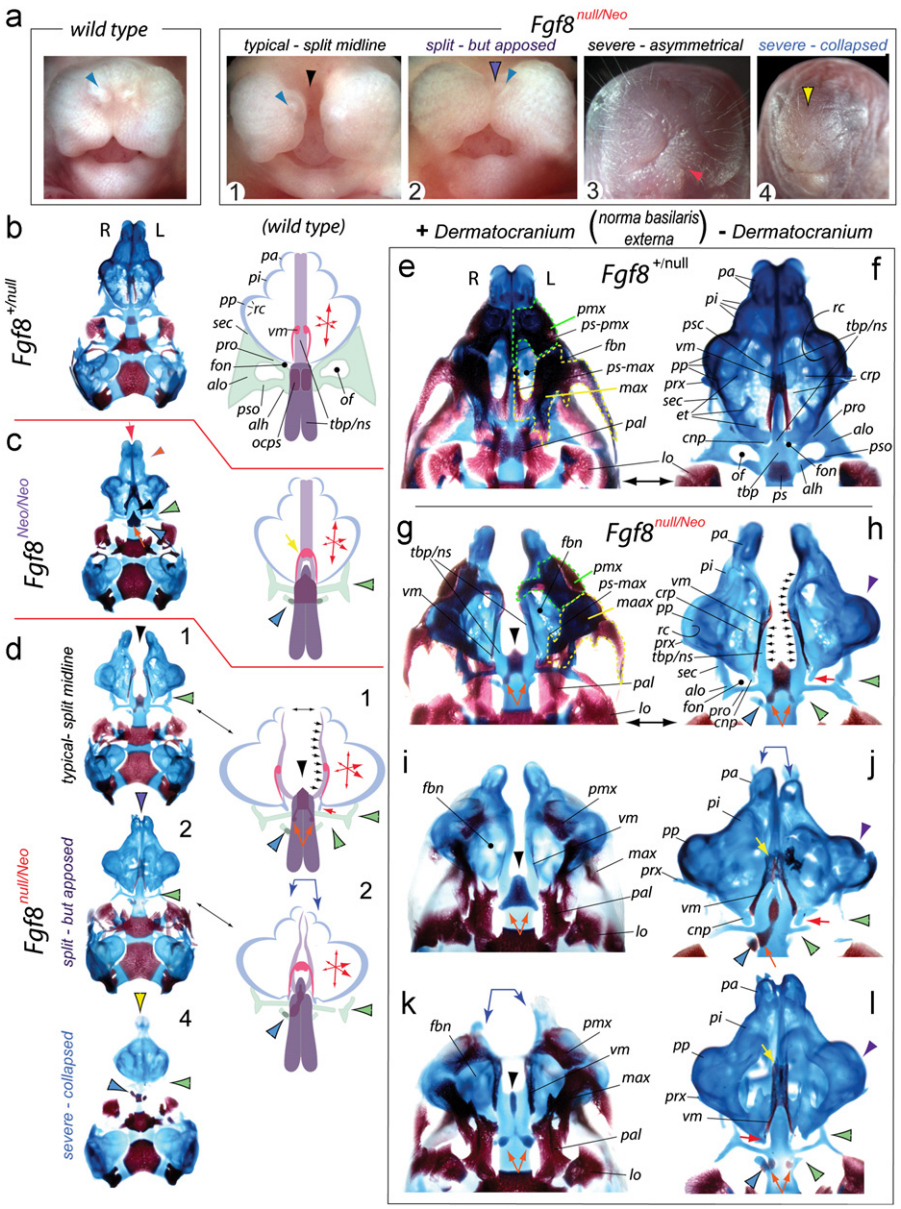

Fig. 2. *Fgf8* is required for inherent, essential mid-facial integration and structural polarity within the NSC and OPC. (a) Gross anatomy of wild-type and $Fgf8^{null/Neo}$ perinates (1–4). Typically ($n=10/14$), mutant embryos had a complete mid-facial cleft (black arrowhead, perinate 1); a few ($n=2/14$) had a clearly split mid-face but some midline facial tissue still apposed (purple-and-black arrowhead, perinate 2). Perinate 3 exhibits an asymmetry of the oral opening (red arrowhead). Rarely ($n=2/14$), $Fgf8^{null/Neo}$ perinates present lack a rhinarium (yellow-and-black arrowhead, perinate 4); such animals exhibit a collapse of structure centered at the midline. Blue arrowheads: external nares. (b)–(l) Demonstration that mid-facial, NSC, and OPC development are sensitive to allelic dosage of *Fgf8* through differential staining of bone (red) and cartilage (blue) in $Fgf8^{+/null}$ (phenotypically wild-type), $Fgf8^{Neo/Neo}$ and $Fgf8^{null/Neo}$ neonatal mice. (b)–(d) Comparison of the skulls of $Fgf8^{+/null}$ (b), $Fgf8^{Neo/Neo}$ (c), and $Fgf8^{null/Neo}$ (d) neonatal mice with diagramatic representations of structural deficits. $Fgf8^{null/Neo}$ skull types correspond numerically to those figured in 'a'. The black arrowhead in 1: typical mid-facial cleft. Purple-and-black arrowhead: the split – but apposed – nature of the midline in mutant 2. Mutant 4, representing the rarest phenotype, has a collapse and loss about the midline such that the contra-lateral capsules meet (yellow-and-black arrowhead). Green-and-black arrowheads indicate OPC deficiencies. Blue-and-black arrowhead: remnants of the precociously ossifying ala hypochiasmatica (alh). Note that the midline (red arrow), NSC (orange-and-purple arrowhead), and OPC (black-and-green arrowhead) defects in the $Fgf8^{Neo/Neo}$ mutants (c), representing the allelic combination with the greatest yield of Fgf8 protein, are less severe than in the $Fgf8^{null/Neo}$ mutants (d). Arrow size in the 'x, y, z coordinate' diagrams of the schemae indicate the relative changes in the polarity of the NSC. Conjoined blue arrows: asymmetry between NSC. (e)–(l) Magnified *norma basalis externa* views of $Fgf8^{+/null}$ (e) and (f) and $Fgf8^{null/Neo}$ (g)–(l) neonatal skulls with either the dermatocranium in situ (left column) or removed (right column). The skulls in 'e' and 'f' are the same specimen; likewise for 'g' and 'h'. The skulls in 'g–i' typify the nature of the mid-facial cleft. Black arrowheads: abnormal rostrad ossification at the midline antero-medial to the ossification centers of the mutant presphenoid (indicated by orange arrows). In mutant NSC, the pars intermedia (pi) and associated premaxillae are hypoplastic while the pars anterior (pa) is even more diminished. The pars posterior (pp; purple arrowheads), however, are enlarged and expanded laterally, containing aberrant turbinalia. Cupola nasi posterior (cnp) are present as just caudal spurs (red arrows). Mutant NSC connect to the NS extensions of the TBP, which, however, is split as it extends from the presphenoid (outlined by the grouped small black arrows in 'd', 'h'). Mutants maintain pre-orbital pillars (pro), but lack elaborated ala orbitali (alo), sphenethmoidal commissures (sec) and post-optic pillars (pso) in their OPC (green-and-black arrowheads). The ala hypochiasmatica at the base of the post-optic pillars are extant and precociously ossified (blue-and-black arrowheads); notably, some asymmetry is evident as the right side ala hypochiasmatica is typically ($n=10/14$) larger and more robust. (For interpretation of the references to color in this figure legend, the reader is referred to the web version of this article).

asymmetry was not noted. Notably, even when asymmetry was encountered these alterations of orientation and polarity were fully penetrant in both contra-lateral NSC in $Fgf8^{null/Neo}$ neonates. Deficits of the cartilaginous NSC were, moreover, mirrored by deficits in the dermatocranial elements associated with them (Fig. 2g), including of the premaxillae and maxillae (which failed to extend palatal shelves). Thus, *Fgf8* regulates the structural polarity of the NSC.

Trabecular basal plate. Both the OPC and NSC of wild-type neonatal skulls are integrated with the chondrocranium through their attachments to the TBP. The TBP is formed from paired midline extensions (trabeculae cranii) running rostrad from the center of the basisphenoid (where the pituitary sits), through the presphenoid and extending rostrad to form the nasal septum between the NSC (Figs. 1 and 2). These paired structures typically condense and chondrify in such a manner that a single midline cartilaginous structure and presphenoidal ossification center is normally seen in skeletal preparations of mice.

The levels of *Fgf8* found in half of the $Fgf8^{Neo/Neo}$ neonates examined ($n=4/8$) were insufficient to generate a completely normal TBP: Ossification of the presphenoid was aberrant and abnormally extended rostrad at the midline where it ended blindly as a gap in the TBP cartilage appeared (Fig. 2c). Rather than extending at the midline from the presphenoid as a single unit, the caudal end of the nasal septum was formed of two struts running rostrad from the lateral margins of the TBP at the pre-optic pillar; the anterior ends of each strut re-met at the midline forming a single, unified nasal septum to which each contra-lateral NSC attached. Vomers, peri-sagittal dermatocranial bones intimately associated with the cartilaginous nasal septum, were present.

Unlike $Fgf8^{Neo/Neo}$ mutants, in typical (cleft) $Fgf8^{null/Neo}$ mutants the nasal septum was clearly and widely split ($n=10/12$), extending branches laterally from the pre-optic pillar (outlined by multiple diminutive black arrows in Fig. 2d, h) that did not meet their contra-lateral partners to form the usual unified midline structure (Fig. 2d, g–i, k). Infrequently ($n=2/12$), the nasal septum was split but each contralateral division closely apposed its opposite (Fig. 2j, l). The body of the mutant presphenoid usually contained three disparate centers of ossification: one each on the lateral margins of the TBP between the ala hypochiasmatica and the pre-optic pillar (Fig. 2g–l) and a third extending rostrad in marked projection at the midline (Fig. 2). Except when the nasal septum were split but apposed ($n=2/12$; Fig. 2j, l), vomers were clearly present along the margins of the widely split nasal septum but did not meet at the midline ($n=10/12$; Fig. 2g–l, k).

Fgf8 dosage determines midfacial structural integration, polarity and orientation within the nasal and optic capsules

Utilizing several combinations of Fgf8 alleles, including $Fgf8^{null/Neo}$, $Fgf8^{Neo/Neo}$ and $Fgf8^{null/wt}$, we have demonstrated that large-scale, consistent (penetrant) differences in cranial skeletal morphologic development occurs in murine perinates carrying disparate combinations of alleles. The consistent, lateral expansion of the pars posterior and enlargement of the recessus cupularis, together with the hypoplasia of the pars anterior (rostrally) and cupola nasi posterior (caudally) (presaged in the skulls of $Fgf8^{Neo/Neo}$ mutants presenting a higher allelic dosage of Fgf8 and given fuller voice in the $Fgf8^{null/Neo}$ mutants constituting a lower Fgf8 dosage) represents a re-orientation of NSC morphogenesis and structure. Moreover, the relative loss of Fgf8 results in an inability to properly consolidate and integrate the TBP (initially two bilateral medial anlage) into a singular, unified midline structure—though it does not eradicate the ability to make midline structures themselves (as witnessed by the presence of NS and vomers). Notably, herein we have provided the first demonstration that Fgf8 is essential for appropriate OPC development and that capsular morphogenesis is Fgf8 dosage sensitive Table 1.

Table 1
Griffin et al.

alh	ala hypochiasmatica
alo	ala orbitalis
ba1	First branchial arch
c	Caudal
CNC	Cranial neural crest
cnp	Cupola nasi posterior
cp	Commissural plate
crp	Cribriform plate
en	External nares
et	Ethmoturbinale
fbn	fenestra basinasalis
FEZ	Facial ectodermal zone
fon	Orbitonasal fissure
fprm	Frontonasal prominence
inc	Incisor
iso	Isthmic organizer
l	Lateral
lFNP	Lateral frontonasal process
lo	Lamina obturans of the alisphenoid
m	Medial
max	Maxillae
md	Mandidular first arch
mFNP	Medial frontonasal process
mol	Molar
mx	Maxillary first arch
na	Nasal
NSC	Nasal capsule
NS/ns	Nasal septum
ocps	Ossification center of the presphenoidodl
odl	Odontogenic line
of	Optic foramen
OFP	Olfactory pit
op	Optic primordia
OP	Olfactory placode
OPC	Optic capsule
pa	Pars anterior of the nasal capsule
pal	Palatine
pi	Pars intermedia of the nasal capsule
pit	Position of the pituitary
pmx	Premaxillae
pp	Pars posterior of the nasal capsule
pro	Pre-optic pillar of optic capsule
ps	Presphenoid
psc	Paraseptal cartilages
ps-max	Palatal shelf of the maxillae
ps-pmx	Palatal shelf of the premaxillae
pso	Post-optic pillar of optic capsule
r	Rostral
rc	Recessus cupularis
Rp	Rathke's pouch
sec	Sphenethmoid commissure
sln	solum nasi
tbp	Trabecular basal plate
trb	Turbinate
vle	Ventro-lateral facial ectoderm
vm	Vomer
vno	Vomeronasal organ
l-lunction	Lambdoidal junction.

$Fgf8^{null/Neo}$ embryos show early embryonic disruption of craniofacial primordia and olfactory pit (OFP) polarity

As analysis of the skulls of $Fgf8^{Neo/Neo}$ and $Fgf8^{null/Neo}$ mutants evinced dosage dependence in capsular (NSC and OPC) and TBP development, we investigated the morphogenetic origins of the craniofacial defects in the more severely affected $Fgf8^{null/Neo}$ embryos through scanning electron microscopy (SEM). SEM permits detailed comparison of the embryonic manifestation of the craniofacial primordia associated with the λ-junction (Tamarin and Boyde, 1977).

From E9.0 to E10, the SCE on either side of the frontal prominence of the normal murine embryo first focally thickens, forming olfactory placodes, and then begins to invaginate centrally. By E10.25, this process results in the formation of an OFP, denoting the future external nares, separating the mFNP and lFNP (Fig. 1 and pseudo-colored green in Fig. 3). Each contra-lateral set of an OFP (This is redundant as 'pseudo-colored green is noted in the previous line), mFNP (pseudo-colored red) and lFNP (pseudo-colored blue), is initially separated by the floor of the frontal prominence and the

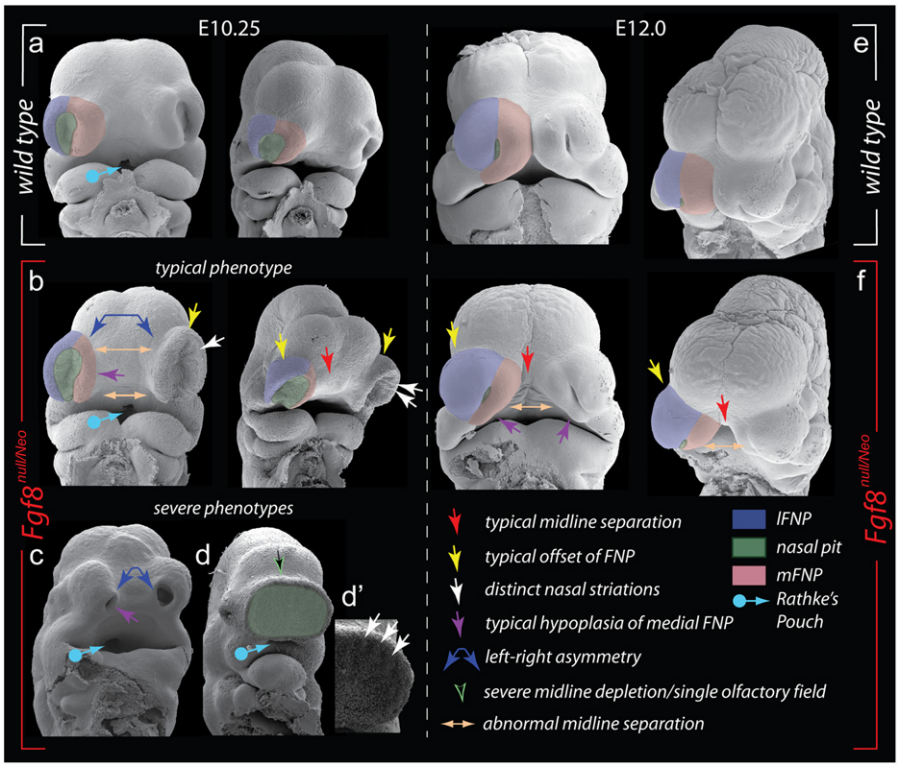

Fig. 3. Scanning electron micrographs of wild-type and *Fgf8*$^{null/Neo}$ embryos document early disruption of craniofacial development and NSC polarity. (a)–(f) Frontal and oblique views of E10.25 (a)–(d′) and E12.0 (e) and (f) wild-type (a), (e) and *Fgf8*$^{null/Neo}$ (b)–(d′), (f) littermate embryos. Key for all figures as indicated in lower right.

roof of the stomodeum: by E12, contra-lateral mFNP meet at the midline to form the so-called intermaxillary segment.

SEM micrographs demonstrated that in *Fgf8*$^{null/Neo}$ embryos, the process of OFP formation was initiated but did not, however, proceed normally (n=5/5): At E10.25, OFP were patent in mutant embryos but they were shallower and greater in breadth both medio-laterally and dorso-ventrally (Fig. 3). Notably, mutant OFP epithelium (n=4/5) developed parallel striations of cells; similar striations were apparent in the most severely affected *Fgf8*$^{null/Neo}$ (one with a single, flattened OFP) (Fig. 3d′). Asymmetry in the size and placement of mutant OFP was occasionally seen (n=2/5). The swelling mFNP and lFNP of the *Fgf8*$^{null/Neo}$ embryos were smaller and larger, respectively, than those found in wild-type embryos and were altogether noticeably offset laterally from the developing head (Fig. 3b).

By E12.0, when compared to wild-type littermates, *Fgf8*$^{null/Neo}$ mutant lFNP were enlarged laterally and mFNP were hypoplastic, in particular where they met the maxillary BA1 and lFNP (n=2/2; Fig. 3f). By this time, the naral openings have normally become small dorso-ventrally oriented slits in the center of the enlarging lFNP and mFNP; mutant nares, however, were shallower, shorter, and mis-oriented obliquely and contra-lateral mFNP failed to appose medially to form intermaxillary segments (Fig. 3f). Together, these alterations correlate with the subsequent mid-facial cleft and the medio-lateral and dorso-ventral re-orientation of NSC morphology seen in *Fgf8*$^{null/Neo}$ neonates.

Fgf8 expression, and that of immediate responsive genes, is lacking in the SCE and FNP of mutant embryos

We investigated whether the levels of Fgf8 in *Fgf8*$^{null/Neo}$ embryos were sufficient for normal embryonic cephalic *Fgf8* expression. At E9.5, normal *Fgf8* expression includes transcripts in the commissural plate, the oral ectoderm of the first branchial arch (BA1), and the ventrolateral ectoderm of the SCE between the commissural plate and the olfactory placode; in mutant embryos, we found moderately decreased transcript levels in BA1, more significant decreases in the commissural plate, and an absence of detectable transcripts in the ventrolateral ectoderm (Fig. 4a). This pattern continued at E10.5 (data not shown). Moreover, frontonasal expression of *Spry1* and *Pea3*, two *Fgf8*-responsive genes (Brent and Tabin, 2004; Firnberg and Neubüser, 2002; McCabe et al., 2006; Minowada et al., 1999; Roehl and Nüsslein-Volhard, 2001), was highly reduced or lost by E10.5 in *Fgf8*$^{null/Neo}$ embryos (Fig. 4b, c).

To determine whether the loss of early ventro-lateral ectoderm *Fgf8* expression in *Fgf8*$^{null/Neo}$ mutant embryos correlated with a potential absence of regional CNC (possibly due to aberrations at the isthmic-organizer; see Trainor et al., 2002), we examined the expression of *Alx3*, a marker of the ectomesenchyme that yields the elements of the frontonasal and TBP skeleton. At E9.5 in *Fgf8*$^{null/Neo}$ embryos, *Alx3* was expressed, in a pattern typical of wild-types, along a ring around the eye and subjacent to the *Fgf8*-less ventro-lateral ectoderm, thus indicating the presence of CNC (Fig. 4d); however, unlike in wild-type embryos, *Alx3*-positive cells were also found at the midline of the stomodeal region of the frontal prominence (Fig. 4d). The presence of regional ectomesenchyme was confirmed with by detection of *Sox9*-positive cells, although in *Fgf8*$^{null/Neo}$ embryos positive cells were detected abnormally ringing the optic primordia (Supplementary Fig. 1a).

Altered polarity of FNP transcription factor expression in Fgf8$^{null/Neo}$ *embryos presages later skeletal defects*

While the decreased dosage of *Fgf8* encountered in typical *Fgf8*$^{null/Neo}$ mutant embryos was found to be insufficient to support normal *Fgf8* expression and signaling in the frontonasal region, it was sufficient to engender invaginating placodes and the subsequent elaboration of medial and lateral FNP swellings: our SEM analysis, however, indicated that, between the advent of

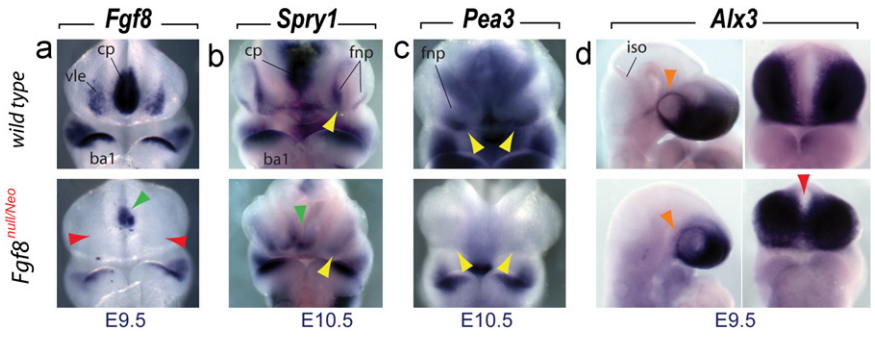

Fig. 4. *Fgf8* and immediate responsive gene expression is lacking during SCE ontogeny. (a) *Fgf8* expression in E9.5 wild-type and *Fgf8*$^{null/Neo}$ littermates. Expression in the commissural plate (cp) is diminished (green arrowhead) while ventro-lateral ectodermal (vle) expression is completely abrogated (red arrowheads). (b) and (c) FNP expression of *Spry1* (b) and *Pea3* (c), two Fgf8-responsive genes, is reduced or lost at E10.5 (compare yellow arrowheads) and weaker in the cp (green arrowhead). (d) Lateral and frontal views of E9.5 wild-type and *Fgf8*$^{null/Neo}$ littermates showing expression of *Alx3*, a marker of the ectomesenchyme yielding the elements of the frontonasal and rostral trabecular skeleton, which is clearly expressed in a ring around the eye (orange arrowheads) and subjacent to the *Fgf8*-less vle, although *Alx3*-positive cells were found ectopically placed across the midline (red arrowhead) in mutants. (For interpretation of the references to color in this figure legend, the reader is referred to the web version of this article).

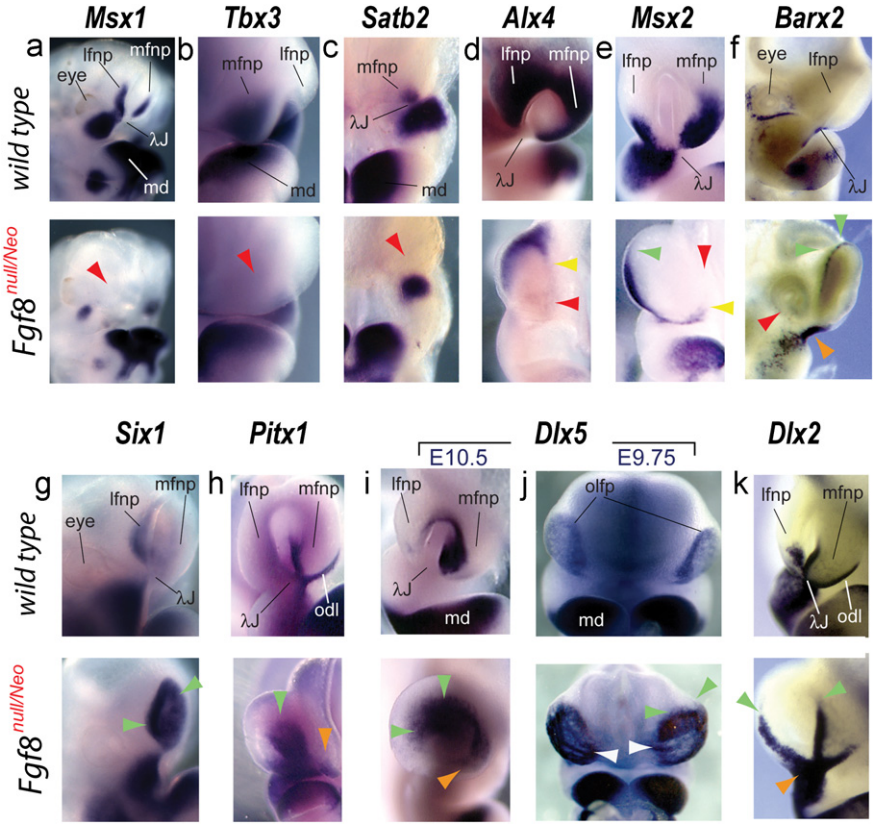

Fig. 5. Altered polarity of transcription factor expression in the frontonasal region presages later skeletal defects. (a)–(k) Comparative in situ hybridization of E10.5 wild-type and *Fgf8*$^{null/Neo}$ littermates. (a) Loss of *Msx1* expression in mutant mFNP and lFNP. (b) and (c) mFNP expression of *Tbx3* (b) and *Satb2* (c) is undetectable in mutant embryos (red arrowheads). (d) *Alx4* transcripts are restricted to the dorso-lateral margins of the flattened OFPs of mutant embryos (yellow arrowhead) and absent in the mFNP (red arrowhead). (e) While diminished, *Msx2* transcripts are expanded toward the dorsal rim of the lFNP (green arrowhead) and ventrally restricted in the mFNP (yellow arrowhead). Red arrowhead: absence in the mFNP core. (f) *Barx2* normally has an unusually punctate expression pattern around the eye and at the λ-junction, but in *Fgf8*$^{null/Neo}$ embryos transcripts are absent around the eye (red arrowhead), increased at the λ-junction (orange arrowhead), and ectopically expressed along the dorsal rim of the OFP (yellow arrowhead). (g) Heightened *Six1* expression (green arrowheads) within the mutant OFP. (h) Lateral expansion of *Pitx1* expression within the mutant OFP (green arrowheads); odontogenic line (odl) expression is more diffuse (orange arrowhead). (i) *Dlx5* expression is expanded laterally within the flattened OFP (green arrowheads). Orange arrowhead: position where vomeronasal primordia would normally arise. (j) At E9.75, *Dlx5* expression is more robust in the *Fgf8*$^{null/Neo}$ OP. Notably, medio-lateral striations of expression are seen (white arrowheads). These striations are similar to those seen in the SEM micrographs in Fig. 3. (k) Maintenance of *Dlx2* transcripts at the mutant center of the λ-junction (orange arrowhead) accompanied by dorsal expansion (green arrowheads) along the OFP rim. (For interpretation of the references to color in this figure legend, the reader is referred to the web version of this article).

placodogenesis and the full maturation of the FNP, regional polarity in the olfactory pit and FNP was affected – with the lFNP expanded and mFNP diminished – in mutant embryos. To molecularly characterize the FNP re-orientation, we analyzed the expression of genes with regionally distinct patterns and known involvement in craniofacial development (Bei and Mass, 1998; Beverdam et al., 2001; Britanova et al., 2006; Compagnucci et al., 2011; Depew et al., 1999, 2002a, 2002b; Depew and Compagnucci, 2008; Depew and Simpson, 2006; Grifone et al., 2005; Han et al., 2007; Lanctôt et al., 1997, 1999; Liu et al., 2005; Qu et al., 1999; Ruf et al., 2004; Satokata et al., 2000; Satokata and Maas, 1994; Schneider et al., 2001;

Szeto et al., 1999; Tucker et al., 1998; Zirzowa et al., 2009; Zou et al., 2004). We were principally interested in understanding the presumptively mature λ-junction at E10.5 as this time-point provides a useful read out of the essential molecular baüplan at the root of subsequent craniofacial morphogenesis (Depew et al., 2002b).

We found that FNP expression patterns in *Fgf8*$^{null/Neo}$ embryos typically fell, relative to wild-type littermates, into one of four categories: (1) complete loss; (2) focal loss (with or without re-orientation); (3) expansion; or (4) relative maintenance. Exemplifying category 1, *Msx1*, *Tbx3* and *Satb2* transcripts were undetectable within the core FNP mesenchyme in *Fgf8*$^{null/Neo}$ embryos (Fig. 5a–c).

Alx4 and *Msx2* are normally expressed in the mFNP and lFNP, where their expression reflects regional dorsal-ventral OFP polarity (with *Alx4* transcripts concentrated dorsally and *Msx2* ventrally). In *Fgf8*$^{null/Neo}$ mutant embryos, expression of both genes was focally lost centrally within the FNP and further restricted dorsally (with *Alx4*) and ventrally (with *Msx2*) (Fig. 5d, e). *Msx2* transcripts were extended dorsally along the lFNP of mutant embryos (Fig. 5e). *Barx2* expression, normally detected in a punctate pattern restricted to the central rami of the λ-junction and posteriorly around the eye, was increased at the central rami, expanded dorsally around the OFP, but lost around the eye in *Fgf8*$^{null/Neo}$ embryos (Fig. 5f).

In addition to dorso-ventral changes, medio-lateral alterations of OFP ectodermal gene expression and intensity of E10.5 *Fgf8*$^{null/Neo}$ embryos was evident, exemplified by the medial-to-lateral expansion in intensity of *Pitx1* and *Dlx5* (Fig. 5h, i). The same was true for the pattern of *Six1* expression, though a degree of asymmetry between contra-lateral FNP was encountered (Fig. 5g and data not shown). More specifically, *Pitx1* expression expanded laterally in the OFP (Fig. 5h). *Pitx1* expression along the odontogenic line of mutant embryos was maintained though it was more diffuse and discontinuous with the center of the λ-junction (Fig. 5h). *Dlx5* expression in *Fgf8*$^{null/Neo}$ embryos abnormally extended laterally at the dorsal end of the mutant OFP but was diminished ventrally (Fig. 5i). At E9.75 (when the OFP are mature, with the underlying mesenchyme beginning to differentially proliferate around them but are not yet invaginating), *Dlx5* expression was increased dorsally and was distinctly seen to line the placode epithelium in striations reminiscent of what was seen in SEM micrographs (Fig. 5j; compare with Fig. 3b, d′). *Dlx2* expression, marking the epithelium at the center of the λ-junction, exemplifies a gene whose core pattern is essentially maintained (but which is expanded dorsally along the FNP) (Fig. 5k). Thus, both dorso-ventral and medio-lateral re-organization of expression patterns defines the λ-junction of *Fgf8*$^{null/Neo}$ mutant embryos.

Transformed topography and polarity of regional signaling systems in the frontonasal region of Fgf8$^{null/Neo}$ *embryos*

Fgf8 has been linked in a dynamic interplay with other regional secreted signaling factors and their effectors. We therefore examined the expressional ontogeny of a number of these factors, including that of *Bmp4*, *Wnt5a* and *Raldh3*.

At E10.25, *Bmp4* expression is normally restricted to the ventral margins of the OFPs at the center of the λ-junction and along the odontogenic line. In typical *Fgf8*$^{null/Neo}$ embryos ventral *Bmp4* expression was maintained though expression abnormally extended dorsad to encompass the entire rim of the mutant OFP: Moreover, mutant embryos evinced an aberrant break in expression between the odontogenic line and the center of the λ-junction (Fig. 6a), and in embryos exhibiting the most severe phenotype no OFP *Bmp4* transcripts were detected (Fig. 6b) but, as with all mutant embryos, were conspicuously prominent in Rathke's pouch.

Numerous *Wnts* are expressed at the λ-junction (Brugmann et al., 2007; Ferretti et al., 2011; Lan et al., 2006), including *Wnt5a* (Yamaguchi et al., 1999). Normally at E10.5, *Wnt5a* transcripts are detected along the rim of the OFP and the lFNP and mFNP cores; we found, however, that *Wnt5a* transcripts were still detected along the rim of the nasal pits of *Fgf8*$^{null/Neo}$ mutant embryos, they were undetected in the FNP cores (Fig. 6c).

Raldh3, a critical component of the regional retinoic acid signaling system, is dynamically expressed in murine embryos from E9 to E10.5 (Dupe et al., 2003). At E10.5, *Raldh3* is conspicuously expressed in a sub-portion of the developing eye and within the invaginated OFP, where it is highly expressed ventrally and weakly expressed dorsally. In *Fgf8*$^{null/Neo}$ mutant embryos at E10.5, *Raldh3* expression is diminished in the optic primordia and expanded dorsally within the OFP (Fig. 6d). Because of its λ-junction centric expression at earlier stages of murine development, we also examined *Raldh3* expression in *Fgf8*$^{null/Neo}$ embryos at E9.25, finding both significant rostral and medial relative extensions in expression (Fig. 6e). Thus, diminished dosages of Fgf8 leads to a regional re-organization of the expression patterns of other secreted signaling factors and their effectors.

Changes are detectable in early optic apoptotic profiles but not in cephalic proliferative profiles in Fgf8$^{null/Neo}$ *murine embryos*

Relative changes in programed cell death and proliferation of the embryonic head of *Fgf8*$^{null/Neo}$ mutant embryos have previously been investigated in the context of telencephalic (Storm et al., 2006) and branchial arch (Abu-Issa et al., 2002) development. We therefore extended these apoptotic and cellular proliferation profiles to include optic and frontonasal embryonic tissues. In accord with a previous report (Storm et al., 2006) we found that, while both the ventral neuroepithelium and the associated SCE overlying the frontal process of the E8.5 *Fgf8*$^{null/Neo}$ mutant embryo contained fewer apoptotic cells than did wild type littermates, there were many more apoptotic cells at the midbrain–hindbrain (isthmic organizer) boundary (Supplementary Fig. 1c). Moreover, at both E9.5 and E10.5, there are greater numbers of apoptotic cells in the mesenchyme surrounding the neuroepithelium of the optic stalk, within the optic stalk itself, and in the ectodermal epithelium associated with the optic primordia (Supplementary Fig. 1b, d, e). We detected only minor differences in the position and number of apoptotic cells associated with developing frontonasal structures (Supplementary Fig. 1). In accord with previous investigations (Abu-Issa et al., 2002; Storm et al., 2006), we failed to detect significant changes in proliferation indexes using anti-phosphohistone H3 antibody assays (Supplementary Fig. 2).

SCE from wild-type and Fgf8$^{null/Neo}$ *murine embryos elicit different responses in xenographs to embryonic chick SCE*

To further test whether reducing the levels of *Fgf8* affects the ability of the ectoderm to regulate patterned growth of frontonasal structures, we utilized a previously characterized mouse–chick chimera system (Hu et al., 2003; Hu and Marcucio, 2009) and transplanted SCE from E10.5 wild-type murine embryos to the dorsal surface of the frontonasal prominence of HH25 stage chick embryos (Fig. 7b). Such transplants result in the formation of both ectopic upper jaw chondrocranial components as well as an associated egg-tooth, an ectodermal appendage used to break out of the shell at hatching (Fig. 7a, c). We found, moreover, that when the ectoderm of an E10-10.5 *Fgf8*$^{null/Neo}$ mutant embryo was transplanted, ectopic upper jaw chondrocranial components, indistinguishable from those

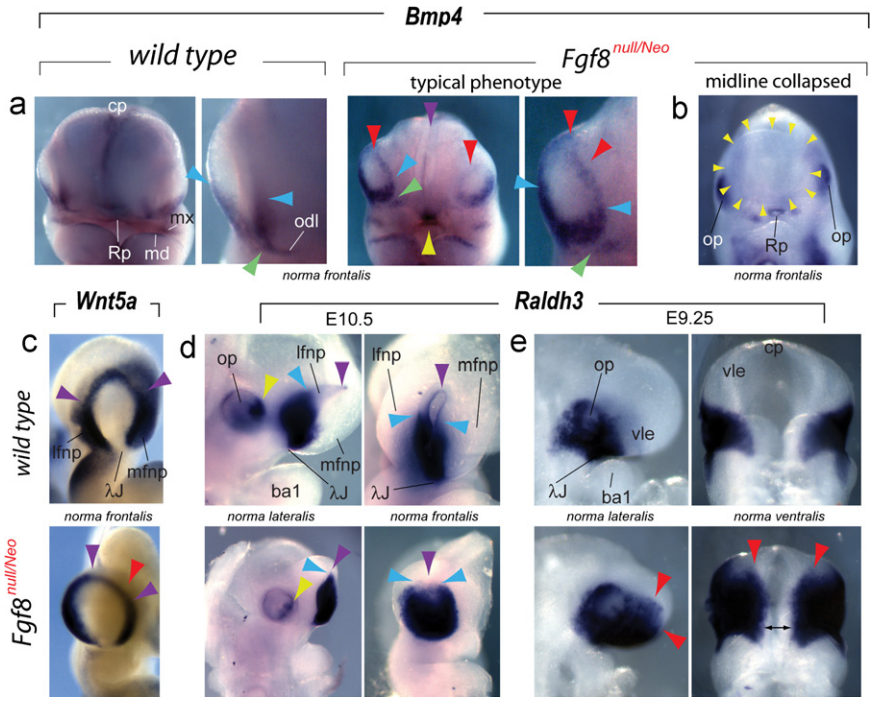

Fig. 6. Transformed topography and polarity of regional signaling systems in the frontonasal region of *Fgf8*$^{null/Neo}$ embryos. (a)–(e) Comparative in situ hybridization. (a) Although *Bmp4* expression at E10.25 is normally restricted to the ventral margins of the OFP at the center of the λ-junction (compare blue arrowheads) and the odontogenic line (odl), in typical *Fgf8*$^{null/Neo}$ embryos *Bmp4* expression extends along the entire rim of the mutant OFP (red arrowheads). Mutant embryos evince a break in *Bmp4* expression between the odl and the center of the λ-junction (compare green arrowheads). Purple arrowhead: decreased expression in the mutant commissural plate (cp). Yellow arrowhead: expression in Rathke's pouch. (b) Lack of detectable *Bmp4* transcripts in the OFP in embryos exhibiting a single, collapsed OFP (yellow arrowheads). (c) *Wnt5a* transcripts are still detected along the rim of the OFP (purple arrowheads) of mutant embryos, though they are diminished in the FNP core (red arrowhead). (d) At E10.5 expression of *Raldh3* is diminished in the optic primordia (compare yellow arrowheads) and expanded dorsally within the OFP of mutant embryos (compare the purple arrowheads, indicating the dorsal rim of the pits, and the blue arrowheads, highlighting the dorsal-most extent of extensive *Raldh3*). (e) At E9.25, *Raldh3* is expanded rostrally (red arrowheads) and medially (double headed black arrow) in mutant embryos. (For interpretation of the references to color in this figure legend, the reader is referred to the web version of this article).

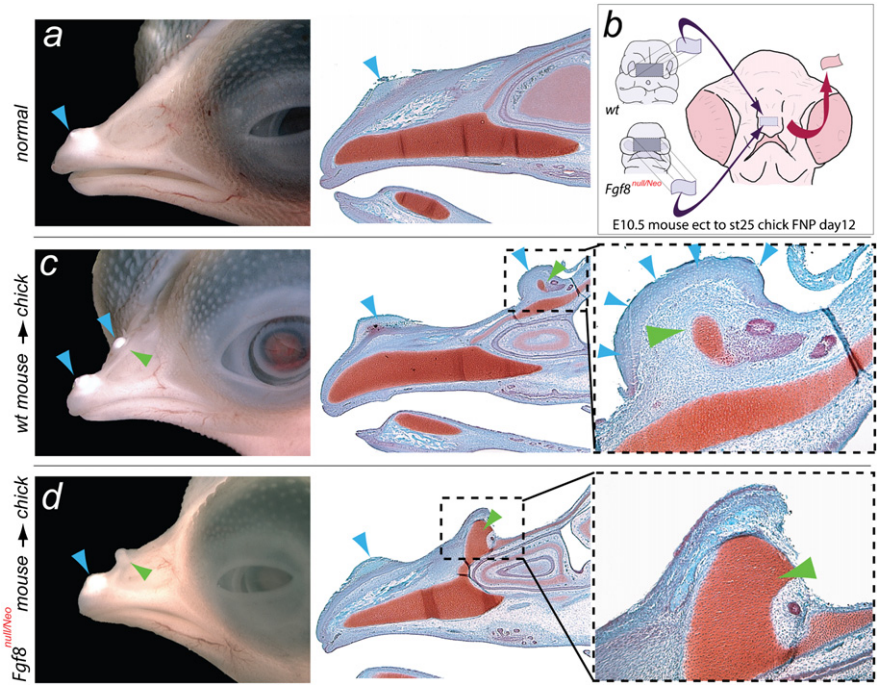

Fig. 7. Differential response to *Fgf8* allelic dosage in murine-chick chimera system for craniofacial ectodermal induction. (a) Lateral view of a normal chick embryo showing the egg-tooth (blue arrowhead) on the dorsal surface of the upper jaw. (b) Diagram of facial ectodermal (FEZ) transplantation from mouse to chick embryo. (c) Transplantation of the FEZ from a wild-type mouse induces duplication of upper jaw structures (green arrowhead, dotted box; magnified to the right). The autochthonous egg-tooth and an ectopic egg-tooth are present in these chimeras (blue arrowheads). (d) Transplantation of the FEZ from an *Fgf8*$^{null/Neo}$ embryo induces duplications of the upper jaw skeleton as in wild-type chimeras, but the mutant FEZ is unable to induce an egg-tooth with the duplicated upper jaw (green arrowhead, dotted box; magnified to the right). (For interpretation of the references to color in this figure legend, the reader is referred to the web version of this article).

induced by a wild-type graft, were likewise found (Fig. 7c, d). Notably, however, ectopic egg-teeth were conspicuously absent. This approach suggests that embryos with different levels of *Fgf8* (i.e., wild-type levels versus hypomorphic levels) generate cephalic ectoderm with disparate inductive competences, and is in line with the idea that *Fgf8* dosage plays a significant role in regional patterning and morphogenesis.

Disscusion

Though complex in structural detail, the skull is constructed on a basic baüplan that contains both dermatocranial (formed of dermal bone) and chondrocranial (cartilaginous) components, each of which can be further subdivided. For instance, the chondrocranium is composed of both splanchnocranial (related to the BA-derived, jaw-forming structures) and neurocranial (related to the support of primary sensory and central nervous system) structures. Although some significant progress has been achieved in understanding the complex patterning mechanisms related to jaw development, less has been achieved in understanding the intricacies of patterning the neurocranial components of the skull. For instance, the otic capsules (OTC), OPC, and NPC of the neurocranium all evince a structural polarity such that each is not simply a symmetric, blind capsule but rather has definitive rostro-caudal, medio-lateral and dorso-ventral axes of structural elaboration (Fig. 1) in which normal functionality is predicated on morphogenesis following these axes. Thus, even small alterations of structural elaboration along these axes potentially bear functional consequences. Patterning mechanisms underlying the structural polarity of the OTC, OPC and NPC, however, largely remain unclarified, as are those regulating how each sensory capsule is integrated (functionally and structurally combined) with the remainder of the neurocranium.

A basic enterprise in evolutionary developmental biological studies of the skull is to understand and detail those patterning mechanisms in play in the manifestation of this cranial structural baüplan as well as in the subsequent elaboration of skeletal form in disparate taxa, accounting for how taxonomic variability in morphology is achieved both ontogenetically and evolutionarily. While it is clear that, mechanistically, the various elaborations of the exquisitely positioned and timed reciprocal cross-talk between the embryonic cephalic epithelia and the subjacent CNC mesenchyme is essential to the development and evolution of the skull, clarifying the initiation, presence, and course of these elaborations (and their ramifications for different levels of patterning of structure at disparate taxonomic levels) is a substantial endeavor, one that underlies the work presented here.

In gnathostomes thus far characterized, *Fgf8* evinces dynamic expression patterns during cephalic epithelial (both neuroepithelial and SCE) ontogeny (Fig. 1). While the elaborate ontogeny of *Fgf8* expression in the cephalic epithelia reflects a dynamic and significant signaling environment to be encountered by the CNC, important particulars of the association of *Fgf8* expression in the cephalic epithelium and subsequent cranial skeletal development and morphogenesis have remained un-determined. Three such areas that have been in need of further understanding include: (1) the possibility that OPC skeletal structures are regulated by *Fgf8*; (2), the nature of *Fgf8* regulation of the NSC; and (3), whether there is a relationship between *levels* of *Fgf8*-associated signaling and the specifics of the complex cranial skeletal patterning, integration, and morphogenesis of structures associated with the λ-junction and TBP.

Murine optic capsulogenesis requires Fgf8

We have presented the first definitive evidence that *Fgf8* is specifically involved with the development of the OPC of the neurocranium. The OPC represent significant embryonic cranial skeletal structures, the molecular patterning particulars of which have been mostly ignored and are largely unknown. As evinced by both $Fgf8^{Neo/Neo}$ ($n=8/8$) and the $Fgf8^{null/Neo}$ ($n=14/14$) neonates, development of both portions of the post-optic pillar are sensitive to *Fgf8* dosage (Fig. 2). Notably, asymmetry between the remnant of the typically larger right and the smaller left ala hypochiasmatica was evident in $Fgf8^{null/Neo}$ neonates ($n=10/14$), being associated with asymmetry in the ossification centers of the presphenoid. Outside of suggesting a possible correlative developmental relationship between the ala hypochiasmatica and the body of the presphenoid, the significance of the aforementioned asymmetries remains unclear (though they potentially derive from early disruption in Fgf8 signaling around gastrulation). Differences between the $Fgf8^{Neo/Neo}$ and $Fgf8^{null/Neo}$ neonates indicate that development of the other components of the optic capsules – the pre-optic pillar and the ala orbitalis – is also sensitive to *Fgf8* dosage.

While a number of other genes expressed in the SCE are known to be required for development of the optic sensory system, the nature of their roles in patterning the supporting optic skeleton are typically less clear. Moreover, the development of the neuronal component of the optic system is apparently not required for optic capsular development, as exemplified by the loss of *Pax6* (Matsuo et al., 1993; Osumi-Yamashita et al., 1997; Compagnucci et al., 2011). While ocular tissue defects likely characterize $Fgf8^{null/Neo}$ mutants, we did not investigate them outside of the skeletal system; we did, however, note changes in gene expression (e.g., *Barx2*, *Sox9*, *Raldh3*) in early optic and peri-ocular cells as well as significant changes in apoptosis in the optic primordia, including in the optic stalk and the surrounding mesenchyme (Supplementary Fig. 1). While it awaits experiments using tissue-specific loss of *Fgf8* to determine whether the OPC defects are directly due to SCE *Fgf8* signaling deficiencies or are perhaps due to defects in *Fgf8* signaling in the developing neuroepithelium (e.g., optic stalk) around which the OPC form, it is now known that *Fgf8* regulates the development of the OPC.

Polarity and orientation within the NSC is sensitive to Fgf8 dosage

Gnathostome NSC vary in structure, being rather simple in chondrichthyans and exquisitely elaborate in olfaction-oriented mammals, though all possess medio-lateral, dorso-ventral and rostro-caudal polarity and the various constituent parts of capsules (such as the turbinalia) and their functionality are elaborated in the context of this polarity.

Extirpation studies indicate that OP epithelium is essential to the formation of the NSC and patterning begins with the specification and initiation of placodogenesis. Though murine *Fgf8* is not required for placodogenesis and OFP invagination, it appears to be required for the subsequent elaboration of the pit into an olfactory-epithelium-containing nasal cavity: inactivation of a floxed allele of *Fgf8* via a $Foxg1^{Cre}$ driver led (Kawauchi et al., 2005) to note that, in mutant mice with such inactivation, OFP formed but that defects in mFNP development were encountered at E10.5. Moreover, the mutant olfactory-epithelium failed to generate appropriate neuronal cell types. *Foxg1*-positive cells are, however, found in most of the SCE, including that associated with the anterior neural ridge (Hébert and McConnell, 2000). As the $Foxg1^{Cre}$ driver is a null allele, a genetic interaction between *Fgf8* and *Foxg1* in these studies cannot be ruled out. Moreover, detailing the consequences for the polarity of structural development of the NSC, or for possible dosage requirements for the cranial skeleton associated with the OP, has not been presented in previous studies.

Both the absolute and the relative sizes of the pars anterior, intermedia and posterior of the NSC (and the turbinalia elaborated therein) are crucial to normal nasal functionality, affecting, for

instance, the relative and absolute surface areas lined with either respiratory or olfactory epithelium. Herein we have provided the first evidence that normal NSC structural orientation, elaboration and polarity – key characteristics of this neurocranial component – are dependent on *Fgf8*. Specifically, we have shown here that decreased dosage of *Fgf8* leads to a caudo-lateral expansion of NSC structure, in particular the pars posterior, at the expense of antero-medial (e.g., the pars anterior) and postero-medial structure (e.g., the cupola nasi posterior). It is important to note that these shifts in structural orientation and polarity were fully penetrant ($n=14/14$), even in those mutants ($n=2/14$) with a midline collapse. Moreover, the small numbers of olfactory foramina further supports the notion that the neuronal component of the olfactory system is compromised in the absence of sufficient Fgf8.

Altered gene expression patterns, corresponding to the structural shifts in normal orientation and polarity of the capsules, are evident in *Fgf8* deficient embryos in both the mesenchyme (*Satb2*, *Spry1*, *Pea3*, *Tbx3*, *Msx1*, and *Msx2*) and the epithelium (*Bmp4*, *Six1*, *Pitx1*, *Dlx5*, and *Raldh3*) of the FNP in E10-E10.5 $Fgf8^{null/Neo}$ mutant embryos. While each of the genes herein described plays a regulatory role in frontonasal development, we bring specific attention to two here. First, the abnormal circum-OFP expression, and disconnect at the odontogenic line, of *Bmp4* in $Fgf8^{null/Neo}$ mutant embryos is a notable exemplar that the signaling environment of the λ-junction itself is re-organized. Second, we emphasize that, as evinced by the rostral and medial expansion of *Raldh3* seen at E9.25, changes in the regional molecular environment are patent prior to the actual advent of the FNP themselves.

Fgf8 and midfacial integration

The shift in the orientation and polarity of the NSC in *Fgf8*-deficient mice is clearly developmentally presaged by changes in the olfactory placode, FNP and OFP. As with $Fgf8^{flox/flox}$; $Foxg1^{Cre}$ embryos presented by Kawauchi et al. (2005), the mFNP is hypoplastic in typical E10.25 $Fgf8^{null/Neo}$ embryos; however, the lFNP is relatively enlarged. These changes are in line with the lateral expansion of NSC structure at the expense of medial structure observed in $Fgf8^{null/Neo}$ perinates. Moreover, the $Fgf8^{null/Neo}$ mutant OFP is characterized by a slight medio-lateral expansion, a decrease in depth, and the presence of neomorphic cellular striations. With the decreased depth of the invagination of the pit of mutant embryos, the elaborated mutant NSC are expanded with respect to deeper structures and diminished in elements closer to the nasal aperture. The OFP epithelial striations are notable, and may indicate a regional change of cellular differentiation and fate; any relationship between the observed change in cellular organization of the OFP and the subsequent changes in capsular orientation and polarity must be further investigated.

$Fgf8^{null/Neo}$ mutant embryos elaborate medially deficient FNP thereby leaving a chasm between the forming nasal apparatuses (Fig. 3). Among the genes depleted in expression in the $Fgf8^{null/Neo}$ mutant FNP is *Alx4* (Fig. 5d), which is notable as *Alx* mutations in humans and mice exhibit mid-facial clefting (Beverdam et al., 2001; Qu et al., 1999; Twigg et al., 2009; Uz et al., 2010). Moreover, based on comparative genomic and expression data, it has been suggested that alteration in *Alx* gene family expression in disparate taxa may have had an impact on regional cranial evolution (McGonnell et al., 2011).

Significantly, despite the presence of a mid-facial cleft ($n=12/14$), midline structures in the form of TBP and their nasal septal extensions – notably associated with dermatocranial vomers – are present in $Fgf8^{null/Neo}$ skulls, and are connected to the re-oriented NSC. Expression of *Satb2* is normally detected in both the mFNP and the maxillary BA1, and its absence in mice leads to the loss of peri-sagittal structures of the NSC—but not to midline TBP structures (Britanova et al., 2006). Its loss in the mFNP in $Fgf8^{null/Neo}$ mutant embryos is thus notable and directly correlates with cranial structural changes evident in mutant neonates. Despite abnormalities in its ossification centers, the presphenoidal portion of the TBP is present: together, these observations suggest that *Fgf8* regulates mid-line *integration* rather than midline *identity* per se (i.e., it regulates the developmental process that causes contra-lateral, medial trabecula cranii to integrate across the midline into one united midline neurocranial structure). It is unclear, however, in what tissue this regulatory *Fgf8* action is centered. For instance, by E9.5 the CNC encounter an abnormal SCE, as indicated by changes in cell markers including *Dlx5, Raldh3*, and *Fgf8* itself; while, the presence of *Alx3*-positive CNC abnormally present at the midline around this time point suggests that normal midline development has been compromised.

Fgf8 dosage dependence in the development of the cranium has not previously been clearly documented, although *Fgf8* dosage dependence in the central nervous system has been noted and occasional variance in midline structural elaboration in $Fgf8^{null/Neo}$ mutants reported (e.g., Storm et al., 2003, 2006). We found that a small percentage of perinatal skulls ($n=2/14$) exhibited a great reduction of midline development (Fig. 2), and we follow previous suggestions that the greater reduction in these infrequent cases is likely due to a failure to meet a threshold level of early Fgf8 signaling.

Fgf8 dosage and the development and evolution of the rostral cranium

The TBP is a CNC-derived midline structure, integrating caudally with the mesodermal parachordal basal plate (at the hypophysis) and extending rostrad as the NS. It thus incorporates the rostral basisphenoid, presphenoid, mesethmoid and nasal septum, and is intimate with the optic and olfactory systems. The cellular dynamics of growth along the TBP are genetically regulated and taxa specific with the number of ossification centers and amount of ossification along its rostro-caudal axis varying between taxa (Barghusen and Hopson, 1979; de Beer, 1985; Broom, 1926, 1927; Goodrich, 1958; Moore, 1981; Depew et al., 2002b). The TBP is integral to the organization of the skull as being, for instance, either platybasic (with a wide basal plate and widely separated orbits) or tropibasic (with a narrow basal plate and close-set orbits) (Barghusen and Hopson, 1979; de Beer, 1985; Goodrich, 1958; Gregory, 1935; Moore, 1981).

How pattern along the TBP is regulated and whether disparate patterning mechanisms exist along its rostro-caudal axis has been unclear. Evidence herein suggests that patterning is disparate along the axis. For instance, midline integration along the TBP between the basisphenoid and the caudal presphenoid is preserved in $Fgf8^{null/Neo}$ mutants while that rostrad from the presphenoid is not—a division closely corresponding to the positioning of the optic system. The abnormal ossification associated with the $Fgf8^{null/Neo}$ presphenoid, including clear peri-sagittal TBP endochondral ossifications at the ala hypochiasmatica and midline extensions between the deviated nasal septa, suggests (1) optic patterning plausibly underlies platybasic and tropibasic distinctions and (2) *Fgf8*-related regulation of the focal, midline initiation of the ossification centers is one factor in the morphogenesis of this region.

It is noteworthy that significant asymmetry of λ-junction associated craniofacial structures has occasionally been selected for during gnathostome evolution. This includes the directional asymmetry of the odontocete cetacean blow-hole (Klima, 1999; Ness, 1967), narwhal tusks (Eales, 1950), unilateral orbits in the Heterosomata (Gregory, 1933), as well as jaw asymmetries in scale-eating cichlids (Hori, 1993; Stewart and Albertson, 2010) and antisymmetric (random sidedness) dental formulae in certain bats (Juste and Ibanez, 1993). Loss-of-function analysis in mice has revealed a number of

genes whose loss results in either directional asymmetries of nasal structures (e.g., *Dlx5*; Depew et al., 1999) or antisymmetric defects (e.g., *Hesx1*; Dattani et al., 1998; *Satb2*; Fish et al., 2011). Our data indicate that the expression patterns of a number of these genes, including of *Dlx5* and *Satb2,* are regulated in part by *Fgf8*. Moreover, we previously noted that, in a subset of neonatal mice in which *Fgf8* was conditionally inactivated in the oral ectoderm, some asymmetric jaw development occurs (Trumpp et al., 1999). Asymmetry in the skulls of *Fgf8* hypomorphic zebrafish has also been subsequently observed (Albertson and Yelick, 2005). Evidence strikingly demonstrates that the naturally occurring, asymmetric skeletal elements of the gnathostomes mentioned above – including those of the NSC, OPC, and jaws – are all regulated in their normal morphology by *Fgf8*. Accumulative data thus places heterotopic, heterochronic or heterofacient regulation of, and by, *Fgf8* at the center of plausible hypotheses regarding the origins of these asymmetries.

Herein we have utilized both genetic and experimental embryologic approaches to vary the levels of Fgf8 in the SCE. These approaches have allowed us to examine graded challenges to *Fgf8*-regulated cranial patterning. Our chimeric xenograft approach demonstrated that embryos with different levels of *Fgf8* (wild-type versus $Fgf8^{null/neo}$) generate cephalic ectoderm with disparate inductive properties and is in line with our murine genetic investigations which show that *Fgf8* dosage plays a significant role in regional patterning and morphogenesis during OPC and NSC development as well as midfacial integration. While these data follow from rather heavy experimental alterations of Fgf8 signaling in embryos, they also indicate the plausibility that selective pressures on regulators of effective Fgf8 mediated signaling are in play during the course of the evolution of the skull. Further clarifying of the initiation, course and regulation of cephalic *Fgf8* expression, together with more thorough evaluation of subsequent Fgf8 protein levels, will shed additional light on the ramifications of Fgf8 signaling for different levels of craniofacial skeletal patterning within and among disparate gnathostome taxa.

Acknowledgments

We thank Gail Martin for the allelic series of *Fgf8* mutant mice and MA Basson, P Crossley, JLR Rubenstein, L Selleri, and P Sharpe for various riboprobe plasmids. MJD thanks Professor Ted Miclau for departmental support, and was funded by the Royal Society, the Dental Institute of King's College London, and Friends of Guy's Hospital. JG and CC were funded by a Marie Curie Early Training Fellowships (MEST-CT-2004-504025). JLF was funded by a HFSP Long Term Fellowship (LT 01061/2007-L).

Appendix A. Supporting information

Supplementary data associated with this article can be found in the online version at http://dx.doi.org/10.1016/j.ydbio.2012.11.014.

References

Abu-Issa, R., Smyth, G., Smoak, I., Yamamura, K., Meyers, E.N., 2002. Fgf8 is required for pharyngeal arch and cardiovascular development in the mouse. Development 129, 4613–4625.

Abzhanov, A., Tabin, C.J., 2004. Shh and Fgf8 act synergistically to drive cartilage outgrowth during cranial development. Dev. Biol. 273, 134–148.

Albertson, R.C., Yelick, P.C., 2005. Roles for fgf8 signaling in left–right patterning of the visceral organs and craniofacial skeleton. Dev. Biol. 283, 310–321.

Bailey, A.P., Bhattacharyya, S., Bronner-Fraser, M., Streit, A., 2006. Lens specification is the ground state of all sensory placodes, from which FGF promotes olfactory identity. Dev. Cell 11, 505–517.

Barghusen, H.R., Hopson, A., 1979. The endoskeleton: the comparative anatomy of the skull and visceral skeleton. In: Wake, M. (Ed.), Hyman's Comparative Anatomy. The University of Chicago Press, Chicago, IL, pp. 265–326.

de Beer, G., 1985. The Development of the Vertebrate Skull. University of Chicago Press, Chicago.

Bei, M., Mass, R., 1998. FGFs and BMP4 induce both Msx1-independent and Msx1-dependent signaling pathways in early tooth development. Development 125, 4325–4333.

Bell, E.T., 1907. Some experiments on the development and regeneration of the eye and nasal organ in frog embryos. Roux's Arch Entwicklungsmech 23, 457–478.

Beverdam, A., Brouwer, A., Reijnen, M., Korving, J., Meijlink, F., 2001. Severe nasal clefting and abnormal embryonic apoptosis in Alx3/Alx4 double mutant mice. Development 128, 3975–3986.

Brent, A.E., Tabin, C.J., 2004. FGF acts directly on the somitic tendon progenitors through the Ets transcription factors Pea3 and Erm to regulate scleraxis expression. Development 131, 3885–3896.

Britanova, O., Depew, M.J., Schwark, M., Thomas, B.L., Miletich, I., Sharpe, P., Tarabykin, V., 2006. Satb2 haploinsufficiency phenocopies 2q32-q33 deletions, whereas loss suggests a fundamental role in the coordination of jaw development. Am. J. Hum. Genet. 79, 668–678.

Broom, R., 1926. On the mammalian presphenoid and mesethmoid bones. Proc. Zool. Soc. 17, 257–264.

Broom, R., 1927. Some further points on the structure of the mammalian basicranial axis. Proc. Zool. Soc. 18, 233.

Brugmann, S.A., Goodnough, L.H., Gregorieff, A., Leucht, P., ten Berge, D., Fuerer, C., Clevers, H., Nusse, R., Helms, J.A., 2007. Wnt signaling mediates regional specification in the vertebrate face. Development 134, 3283–3295.

Burr, H.S., 1916. The effects of the removal of the nasal pits in Amblystoma embryos. J. Exp. Zool. 20, 27–51.

Compagnucci, C., Fish, J.L., Schwark, M., Tarabyki, V., Depew, M.J., 2011. Pax6 regulates craniofacial form through its control of an essential cephalic ectodermal patterning center. Genesis 49, 307–325.

Corsin, J., 1971. Influences des placodes olfactives et des ebauches optiques sur la morphogenese du squelette cranien chez Pleurodeles waltlii Michach. Annales d'Embryologie et de Moerphogenese 1, 41–48.

Crossley, P.H., Martin, G.R., 1995. The mouse Fgf8 gene encodes a family of polypeptides and is expressed in regions that direct outgrowth and patterning in the developing embryo. Development 121, 439–451.

Creuzet, S., Schuler, B., Couly, G., Le Douarin, N.M., 2004. Reciprocal relationships between Fgf8 and neural crest cells in facial and forebrain development. Proc. Natl. Acad. Sci. USA 101, 4843–4847.

Dattani, M.T., Martinez-Barbera, J.P., Thomas, P.Q., Brickman, J.M., Gupta, R., Martensson, I.L., Toresson, H., Fox, M., Wales, J.K., Hindmarsh, P.'.C., Krauss, S., Beddington, R.S., Robinson, I.C., 1998. Mutations in the homeobox gene HESX1/Hesx1 associated with septo-optic dysplasia in human and mouse. Nat. Genet. 19, 125–133.

Depew, M.J., Liu, J.K., Long, J.E., Presley, R., Meneses, J.J., Pedersen, R.A., Rubenstein, J.L., 1999. Dlx5 regulates regional development of the branchial arches and sensory capsules. Development 126, 3831–3846.

Depew, M.J., Lufkin, T., Rubenstein, J.L.R., 2002a. Specification of jaw subdivisions by Dlx genes. Science 298, 381–385.

Depew, M.J., Tucker, A.S., Sharpe, P.T., 2002b. In: Rossant, J., Tam, P. (Eds.), Craniofacial Development. In: Mouse Development: Patterning, Morphogenesis, and Organogenesis. Academic Press, London, pp. 421–498.

Depew, M.J., Simpson, C.A., 2006. 21st century neontology and the comparative development of the vertebrate skull. Dev. Dyn. 235, 1256–1291.

Depew, M.J., 2008. Analysis of Skeletal Ontogenesis through Differential Staining of Bone and Cartilage. Methods Mol. Biol. 46, 37–45.

Depew, M.J., Compagnucci, C., 2008. Tweaking the hinge and caps: testing a model of the organization of jaws. J. Exp. Zool. 310B, 315–335.

Dode, C., Hardelin, J.P., 2009. Kallmann syndrome. Eur. J. Hum. Genet. 17, 139–146.

Dupe, V., Matt, N., Garnier, J.M., Chambon, P., Mark, M., Ghyselinck, N.B., 2003. A newborn lethal defect due to inactivation of retinaldehyde dehydrogenase type 3 is prevented by maternal retinoic acid treatment. Proc. Natl. Acad. Sci. USA 100, 14036–14041.

Eales, N.B., 1950. The skull of the foetal narwhal, *Monodon monoceros* L. Phil. Trans. Roy. Soc. London, B 235, 1–33.

Ferguson, C.A., Tucker, A.S., Sharpe, P.T., 2000. Temporospatial cell interactions regulating mandibular and maxillary arch patterning. Development 127, 403–412.

Ferretti, E., Li, B., Zewdu, R., Wells, V., Hebert, J.M., Karner, C., Anderson, M.J., Williams, T., Dixon, J., Dixon, M.J., Depew, M.J., Selleri, L., 2011. A conserved Pbx-Wnt-p63-Irf6 regulatory module controls face morphogenesis by promoting epithelial apoptosis. Dev. Cell 21, 627–641.

Firnberg, N., Neubüser, A., 2002. FGF signaling regulates expression of Tbx2, Erm, Pea3, and Pax3 in the early nasal region. Dev. Biol. 247, 237–250.

Fish, J., Villmoare, B., Kobernick, K., Compagnucci, C., Britanova, O., Tarabykin, V., Depew, M.J., 2011. Satb2, modularity, and the evolvability of the vertebrate jaw. Evol. Dev. 13, 549–564.

Frank, D.U., Fotheringham, L.K., Brewer, J.A., Muglia, L.J., Tristani-Firouzi, M., Capecchi, M.R., Moon, A.M., 2002. An Fgf8 mouse mutant phenocopies human 22q11 deletion syndrome. Development 129, 4591–4603.

Goodrich, E.S., 1958. Studies on the Structure and Development of Vertebrates. Dover Publications, New York.

Gregory, W.K., 1933. Fish skulls: a study of the evolution of natural mechanisms. Transactions of the American Philosophical Society 23, 75–481.

Gregory, W.K., 1935. Williston's law' relating to the evolution of skull bones in the vertebrates. Am. J. Phys. Anthropol. 20, 123–152.
Grifone, R., Demignon, J., Houbron, C., Souil, E., Niro, C., Seller, M.J., Hamard, G., Maire, P., 2005. Six1 and Six4 homeoproteins are required for Pax3 and Mrf expression during myogenesis in the mouse embryo. Development 132, 2235–2249.
Han, J., Ishii, M., Bringas, P., Maas, R.L., Maxson, R.E., Chai, Y., 2007. Concerted action of Msx1 and Msx2 in regulating cranial neural crest cell differentiation during frontal bone development. Mech. Dev. 124, 729–745.
Hébert, J.M., McConnell, S.K., 2000. Targeting of cre to the Foxg1 BF-1. locus mediates loxP recombination in the telencephalon and other developing head structures. Dev. Biol. 222, 296–306.
Hori, M., 1993. Frequency-dependent natural selection in the handedness of scale-eating cichlid fish. Science 260, 216–219.
Hu, D., Marcucio, R.S., Helms, J.A., 2003. A zone of frontonasal ectoderm regulates patterning and growth in the face. Development 130, 1749–1758.
Hu, D., Marcucio, R.S., 2009. A SHH-responsive signaling center in the forebrain regulates craniofacial morphogenesis via the facial ectoderm. Development 136, 107–116.
Juste, J., Ibanez, C., 1993. An asymmetric dental formula in a mammal, the Sao Tome Island fruit bat Myonycteris brachyceplala Mammalia: Megacchiroptera. Can. J. Zool. 71, 221–224.
Kawauchi, S., Shou, J., Santos, R., Hébert, J.M., McConnell, S.K., Mason, I., Calof, A.L., 2005. Fgf8 expression defines a morphogenetic center required for olfactory neurogenesis and nasal cavity development in the mouse. Development 132, 5211–5223.
Klima, M., 1999. Development of the cetacean nasal skull. Adv. Anat. Embryol. Cell. Biol. 149, 1–143.
Lan, Y., Ryan, R.C., Zhang, Z., Bullard, S.A., Bush, J.O., Maltby, K.M., Lidral, A.C., Jiang, R., 2006. Expression of Wnt9b and activation of canonical Wnt signaling during midfacial morphogenesis in mice. Dev. Dyn. 235, 1448–1454.
Lanctôt, C., Lamolet, B., Drouin, J., 1997. The bicoid-related homeoprotein Ptx1 defines the most anterior domain of the embryo and differentiates posterior from anterior lateral mesoderm. Development 124, 2807–2817.
Lanctôt, C., Moreau, A., Chamberland, M., Tremblay, M.L., Drouin, J., 1999. Hindlimb patterning and mandible development require the Ptx1 gene. Development 126, 1805–1810.
Lioubinski, O., Alonso, M.T., Alvarez, Y., Vendrell, V., Garrosa, M., Murphy, P., Schimmang, T., 2006. FGF signalling controls expression of vomeronasal receptors during embryogenesis. Mech. Dev. 123, 17–23.
Liu, W., Sun, X., Braut, A., Mishina, Y., Behringer, R.R., Mina, M., Martin, J.F., 2005. Distinct functions for Bmp signaling in lip and palate fusion in mice. Development 132, 1453–1461.
Macatee, T.L., Hammond, B.P., Arenkiel, B.R., Francis, L., Frank, D.U., Moon, A.M., 2003. Ablation of specific expression domains reveals discrete functions of ectoderm- and endoderm-derived FGF8 during cardiovascular and pharyngeal development. Development 130, 6361–6374.
Marcucio, R.S., Cordero, D.R., Hu, D., Helms, J.A., 2005. Molecular interactions coordinating the development of the forebrain and face. Dev. Biol. 284, 48–61.
Matsuo, T., Osumi-Yamashita, N., Noji, S., Ohuchi, H., Koyama, E., Myokai, F., Matsuo, N., Taniguchi, S., Doi, H., Iseki, S., Ninomiya, Y., Fujiwara, M., T. Watanabe, T., Eto, K., 1993. A mutation in the Pax-6 gene in rat small eye is associated with impaired migration of midbrain crest cells. Nat. Genet. 3, 299–304.
McCabe, K.L., McGuire, C., Reh, T.A., 2006. Pea3 expression is regulated by FGF signaling in developing retina. Dev. Dyn. 235, 327–335.
McGonnell, I.M., Graham, A., Richardson, J., Fish, J.L., Depew, M.J., Dee, C.T., Holland, P.W.H., Takahashie, T., 2011. Evolution of the Alx homeobox gene family: parallel retention and independent loss of the vertebrate Alx3 gene. Evol. Dev. 13, 343–351.
Meyers, E.N., Lewandoski, M., Martin, G.R., 1998. An Fgf8 mutant allelic series generated by Cre- and Flp-mediated recombination. Nat. Genet. 18, 136–141.
Minowada, G., Jarvis, L., Chi, C.L., Neubüser, A., Sun, X., Hacohen, N., Krasnow, M.A., Martin, G.R., 1999. Vertebrate Sprouty genes are induced by FGF signaling and can cause chondrodysplasia when overexpressed. Development 126, 4465–4475.
Moore, W.J., 1981. The Mammalian Skull. Cambridge University Press, Cambridge, UK.
Ness, A.R., 1967. A measure of asymmetry of the skulls of odontocete whales. J. Zool. 153, 209–221.
Neubüser, A., Peters, H., Balling, R., Martin, G.R., 1997. Antagonistic interactions between FGF and BMP signaling pathways: a mechanism for positioning the sites of tooth formation. Cell 90, 247–255.
Osumi-Yamashita, N., Kuratani, S., Ninomiya, Y., Aoki, K., Iseki, S., Chareonvit, S., Doi, H., Fujiwara, M., Watanabe, T., Eto, K., 1997. Cranial anomaly of homozygous rSey rat is associated with a defect in the migration pathway of midbrain crest cells. Dev. Growth Differ. 39, 53–67.
Pauws, E., Stanier, P., 2007. FGF signalling and SUMO modification: new players in the aetiology of cleft lip and/or palate. Trends Genet. 23, 631–640.
Qu, S., Tucker, S.C., Zhao, Q., deCrombrugghe, B., Wisdom, R., 1999. Physical and genetic interactions between Alx4 and Cart1. Development 126, 359–369.
Reiss, J.O., 1998. Anuran postnasal wall homology: an experimental extirpation study. J. Morphol. 238, 343–353.
Riley, B.M., Mansilla, M.A., Ma, J., Daack-Hirsch, S., Maher, B.S., Raffensperger, L.M., Russo, E.T., Vieira, A.R., Dodé, C., Mohammadi, M., Marazita, M.L., Murray, J.C., 2007. Impaired FGF signaling contributes to cleft lip and palate. Proc. Natl. Acad. Sci. USA 104, 4512–4517.
Roehl, H., Nüsslein-Volhard, C., 2001. Zebrafish pea3 and erm are general targets of FGF8 signaling. Curr. Biol. 11, 503–507.
Ruf, R.G., Xu, P.X., Silvius, D., Otto, E.A., Beekmann, F., Muerb, U.T., Kumar, S., Neuhaus, T.J., Kemper, M.J., Raymond Jr, R.M., Brophy, P.D., Berkman, J., Gattas, M., Hyland, V., Ruf, E.M., Schwartz, C., Chang, E.H., Smith, R.J., Stratakis, C.A., Weil, D., Petit, C., Hildebrandt, F., 2004. SIX1 mutations cause branchio-oto-renal syndrome by disruption of EYA1-SIX1-DNA complexes. Proc. Natl. Acad. Sci. USA 101, 8090–8095.
Satokata, I., Ma, L., Ohshima, H., Bei, M., Woo, I., Nishizawa, K., Maeda, T., Takano, Y., Uchiyama, M., Heaney, S., Peters, H., Tang, Z., Maxson, R., Maas, R., 2000. Msx2 deficiency in mice causes pleiotropic defects in bone growth and ectodermal organ formation. Nat. Genet. 24, 391–395.
Satokata, I., Maas, R., 1994. Msx1 deficient mice exhibit cleft palate and abnormalities of craniofacial and tooth development. Nat. Genet. 6, 348–356.
Schmalhausen, O.I., 1939. Role of the olfactory sac in the development of the cartilage capsule of the olfactory organ in Urodela. Dokl. Akad. Nauk. SSSR 23, 395–397.
Schneider, R.A., Hu, D., Rubenstein, J.L., Maden, M., Helms, J.A., 2001. Local retinoid signaling coordinates forebrain and facial morphogenesis by maintaining FGF8 and SHH. Development 128, 2755–2767.
Stewart, T.A., Albertson, R.C., 2010. Evolution of a unique predatory feeding apparatus: functional anatomy, development and a genetic locus for jaw laterality in Lake Tanganyika scale-eating cichlids. BMC Biology 8, 8.
Storm, E.E., Rubenstein, J.L., Martin, G.R., 2003. Dosage of Fgf8 determines whether cell survival is positively or negatively regulated in the developing forebrain. Proc. Natl. Acad. Sci. USA 100, 1757–1762.
Storm, E.E., Garel, S., Borello, U., Hebert, J.M., Martinez, S., McConnell, S.K., Martin, G.R., Rubenstein, J.L., 2006. Dose-dependent functions of Fgf8 in regulating telencephalic patterning centers. Development 133, 1831–1844.
Sun, X., Meyers, E.N., Lewandoski, M., Martin, G.R., 1999. Targeted disruption of Fgf8 causes failure of cell migration in the gastrulating mouse embryo. Genes. Dev. 13, 1834–1846.
Szabo-Rogers, H.L., Geetha-Loganathan, P., Nimmagadda, S., Fu, K.K., Richman, J.M., 2008. FGF signals from the nasal pit are necessary for normal facial morphogenesis. Dev. Biol. 318, 289–302.
Szeto, D.P., Rodriguez-Esteban, C., Ryan, A.K., O'Connell, S.M., Liu, F., Kioussi, C., Gleiberman, A.S., Izpisua-Belmonte, J.C., Rosenfeld, M.G., 1999. Role of the Bicoid-related homeodomain factor Pitx1 in specifying hindlimb morphogenesis and pituitary development. Genes. Dev. 13, 484–494.
Tamarin, A., Boyde, A., 1977. Facial and visceral arch development in the mouse embryo: a study by scanning electron microscopy. J. Anat. 124, 563–580.
Toerien, M.J., Roussouw, R.J., 1977. Experimental studies on the origins of the parts of the nasal capsule. S. Afr. J. Sci. 73, 371–374.
Trainor, P.A., Ariza-McNaughton, L., Krumlauf, R., 2002. Role of the isthmus and FGFs in resolving the paradox of neural crest plasticity and prepatterning. Science 295, 1288–1291.
Trumpp, A., Depew, M.J., Rubenstein, J.L., Bishop, J.M., Martin, G.R., 1999. Cre-mediated gene inactivation demonstrates that FGF8 is required for cell survival and patterning of the first branchial arch. Genes. Dev. 13, 3136–3148.
Tucker, A.S., Al Khamis, A., Sharpe, P.T., 1998. Interactions between Bmp-4 and Msx-1 act to restrict gene expression to odontogenic mesenchyme. Dev. Dyn. 212, 533–539.
Tucker, A.S., Al Khamis, A., Ferguson, C.A., Bach, I., Rosenfeld, M.G., Sharpe, P.T., 1999a. Conserved regulation of mesenchymal gene expression by Fgf-8 in face and limb development. Development 126, 221–228.
Tucker, A.S., Yamada, G., Grigoriou, M., Pachnis, V., Sharpe, P.T., 1999b. Fgf-8 determines rostral-caudal polarity in the first branchial arch. Development 126, 51–61.
Twigg, S.R., Versnel, S.L., Nürnberg, G., Lees, M.M., Bhat, M., Hammond, P., Hennekam, R.C., Hoogeboom, A.J., Hurst, J.A., Johnson, D., Robinson, A.A., Scambler, P.J., Gerrelli, D., Nürnberg, P., Mathijssen, I.M., Wilkie, A.O., 2009. Frontorhiny, a distinctive presentation of fronto- nasal dysplasia caused by recessive mutations in the ALX3 homeobox gene. Am. J. Hum. Genet. 84, 698–705.
Uz, E., Alanay, Y., Aktas, D., Vargel, I., Gucer, S., Tuncbilek, G., von Eggeling, F., Yilmaz, E., Deren, O., Posorski, N., Ozdag, H., Liehr, T., Balci, S., Alikasifoglu, M., Wollnik, B., Akarsu, N.A., 2010. Disruption of ALX1 causes extreme microphthalmia and severe facial clefting: expanding the spectrum of autosomal-recessive ALX-related frontonasal dysplasia. Am. J. Hum. Genet. 86, 789–796.
Yamaguchi, T.P., Bradley, A., McMahon, A.P., Jones, S., 1999. A Wnt5a pathway underlies outgrowth of multiple structures in the vertebrate embryo. Development 126, 1211–1223.
Zirzowa, S., Lüdtkea, T.H.W., Bronsb, J.F., Petrya, M., Christoffelsb, V.M., Kispert, A., 2009. Expression and requirement of T-box transcription factors Tbx2 and Tbx3 during secondary palate development in the mouse. Dev. Biol. 336, 145–155.
Zwilling, E., 1940. An experimental analysis of the development of the anuran olfactory organ. J. Exp. Zool. 84, 291–323.
Zou, D., Silvius, D., Fritzsch, B., Xu, P.X., 2004. Eya1 and Six1 are essential for early steps of sensory neurogenesis in mammalian cranial placodes. Development 131, 5561–5572.